

# Characterisation and modelling of the cured shapes of arbitrary layup bistable composite laminates

David N. Betts<sup>a,\*</sup>, Aki I.T. Salo<sup>b</sup>, Christopher R. Bowen<sup>a</sup>, Hyunsun A. Kim<sup>a</sup>

<sup>a</sup>Department of Mechanical Engineering, University of Bath, Bath, BA2 7AY, United Kingdom

<sup>b</sup>Sport and Exercise Science, University of Bath, Bath, BA2 7AY, United Kingdom

## ARTICLE INFO

### Article history:

Available online 11 December 2009

### Keywords:

Composite laminates  
Asymmetric  
Bistable  
Modelling  
Three-dimensional analysis

## ABSTRACT

Asymmetric laminates can have a bistable response to loading, making them of particular interest for applications requiring a large deflection with relatively small and removable energy input. After nearly 30 years of research effort the effects of ply orientation and laminate geometry on the room-temperature shapes of such laminates are well understood and the temperature dependent deformations of laminates of arbitrary layup can be quantitatively predicted. With attention switching to the design of mechanisms incorporating bistable laminates for actuation there is an increasing importance placed on the accuracy and the sensitivity of modelling techniques to predict out-of-plane deflections. This paper presents the results of a novel experimental investigation to map the surface profiles of a series of arbitrary layup laminates. It is concluded that while existing modelling techniques are successful in accurately predicting room-temperature shapes, the sensitivity of solutions to imperfections is significant.

© 2009 Elsevier Ltd. All rights reserved.

## 1. Introduction

It is well known that asymmetric laminates can have multiple equilibrium states in which continuous energy input is not required to maintain a structural shape [1]. Asymmetric laminates have an anisotropic response to the elevated temperatures experienced during manufacture, and the residual thermal stress leads to a curved deformation. Such a curved laminate can have two stable states at room-temperature, with a state change achievable by applying an in-plane strain. These characteristics are of particular interest in applications requiring large deflections with relatively small energy input, such as aerospace applications. For example, a [0/90] laminate can have two approximately cylindrical room-temperature configurations with equal and opposite major curvature in the  $x$ - and  $y$ -directions, Fig. 1a and b, respectively. A saddle shape third equilibrium state, Fig. 1c, is also indicated by modelling [2] but shown to be unstable. For a laminate of this type the two stable cylindrical shapes have equal total potential energy. Each configuration is therefore equally likely to exist, with only small imperfections in material and manufacturing dictating the existence of one shape over the other. Such bistable behaviour of cross-ply laminates has been extensively studied experimentally and well characterised [2–5].

However, fewer studies have been seen in the characterisation of laminates with layups differing from the [0/90] case, referred

to here as having an ‘arbitrary’ layup. For example, a [−30/60] laminate exhibits similar characteristics to a [0/90] laminate. Two cylindrical room-temperature shapes are observed, Fig. 2a and b, with equal and opposite curvature in the  $x$ - and  $y$ -directions. However, due to the off-axis fibre directions the principal curvature is no longer aligned with the global axes. An unstable saddle shape equilibrium state, Fig. 2c, is again indicated by modelling.

There have been a number of attempts to model the shapes and the bistable behaviour of arbitrary layup laminates [6–9]. Dang and Tang [6] generalised Hyer’s original cross-ply model [2] to predict the room-temperature shapes of asymmetric laminates of arbitrary layup based on assumed displacements. Both Hyer [2] and Dang and Tang [6] included the assumption that in-plane shear strain is zero. Jun and Hong [4] investigated the effect of this residual shear strain and found it to be significant in the range of medium width-to-thickness ratio around the bifurcation point. Subsequent modelling developments tend to allow non-zero in-plane shear strain. Jun and Hong [7] further modified the model by including additional polynomial terms to the displacement functions, resulting in generalised expressions with increased complexity. Limited experimental comparisons of the angle of principal curvature were presented and no results were presented to quantify the principal curvatures.

Later work by Dano and Hyer [8] approached the modelling differently, directly using approximations of the midplane strains rather than displacements. Experimental studies were compared to an ideal modelling condition, capturing the general shape and displacements with some discrepancies in both magnitude and

\* Corresponding author. Tel.: +44 (0)1225 385558.  
E-mail address: [en3db@bath.ac.uk](mailto:en3db@bath.ac.uk) (D.N. Betts).

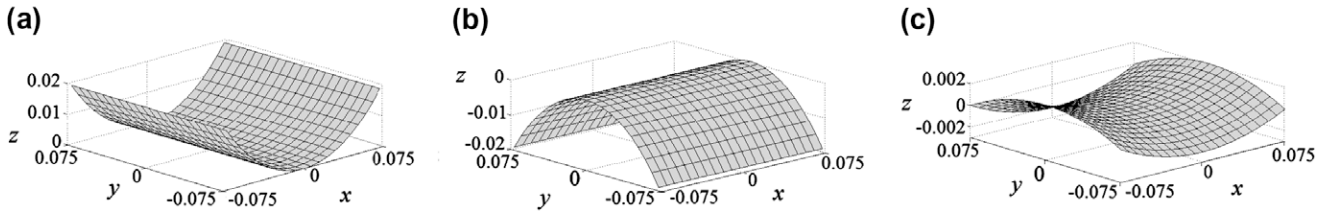


Fig. 1. Room-temperature shapes of a square [0/90] laminate: (a) stable cylindrical shape, (b) opposite cylindrical shape, and (c) unstable saddle shape.

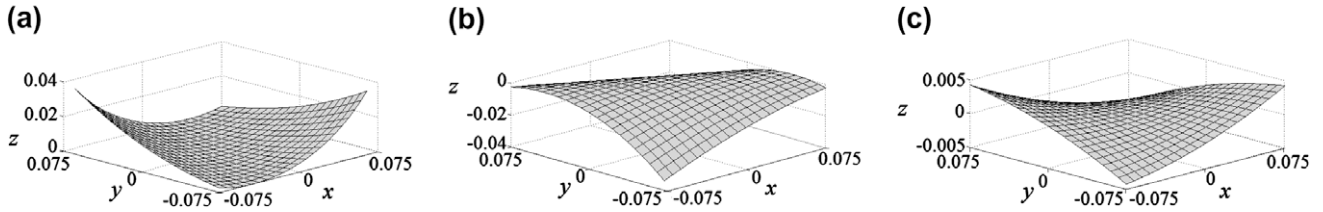


Fig. 2. Room-temperature shapes of a square [-30/60] laminate: (a) stable cylindrical shape, (b) opposite cylindrical shape, and (c) unstable saddle shape.

angle of principal curvature. Finite element (FE) modelling was used to validate the results, demonstrating very similar errors to the analytical model when compared to experimental data. Ren [10] extended this FE validation with the inclusion of a piezoelectric patch to the surface of the laminate. Results showed good correlation between finite element modelling and analytical modelling.

Hamamoto and Hyer [3] demonstrated the significant nature of imperfections on the shapes and bistable behaviour of cross-ply laminates. The influence of a rough resin surface was studied by Giddings et al. [11] by modelling an imperfect laminate using FE. Results demonstrated that good agreement can be achieved between FE and experimental results, given an accurate definition of the laminate structure.

The aim of this work was to compare the experimentally observed shapes of a series of laminates with arbitrary layup to the predictions of existing modelling techniques and study the uncertainties of the analytical model. This paper presents a novel experimental technique to capture the room-temperature profiles of bistable asymmetric laminates. Discrepancies between experimental and theoretical results are discussed. These errors are considered in a quantitative discussion of factors known to influence the room-temperature shapes, highlighting the limitations of existing modelling methods.

## 2. Analytical model

The model for the shapes of asymmetric bistable laminates used in this paper was introduced by Dano and Hyer [8], and has been verified against experimental and FE results [8–10]. This model is based on a nonlinear extension to classical laminated plate theory (CLT) with the approximated midplane strain functions and non-zero in-plane shear strain. A Rayleigh–Ritz method of minimisation of the total strain energy of a laminate is used to obtain information defining the room-temperature shapes. This model is briefly outlined in this section.

The co-ordinate system used is that defined in Fig. 1. The origin sits at the geometric centre of the laminate and plies are defined in order starting from the top surface. The displacement in the  $z$ -direction,  $w$ , is assumed to be of the form

$$w(x, y) = 0.5(ax^2 + by^2 + cxy) \quad (1)$$

The midplane strains are defined as

$$\begin{aligned} \varepsilon_x^0 &= \frac{\partial u^0}{\partial x} + \frac{1}{2} \left( \frac{\partial w}{\partial x} \right)^2 \\ \varepsilon_y^0 &= \frac{\partial v^0}{\partial y} + \frac{1}{2} \left( \frac{\partial w}{\partial y} \right)^2 \\ \varepsilon_{xy}^0 &= \frac{\partial u^0}{\partial y} + \frac{\partial v^0}{\partial x} + \frac{\partial w}{\partial x} \frac{\partial w}{\partial y} \end{aligned} \quad (2)$$

where geometrical nonlinearity is included according to the von Karman hypothesis. The curvatures  $\kappa$ , are defined as

$$\begin{aligned} \kappa_x &= -\frac{\partial^2 w}{\partial x^2} = -a \\ \kappa_y &= -\frac{\partial^2 w}{\partial y^2} = -b \\ \kappa_{xy} &= -2\frac{\partial^2 w}{\partial x \partial y} = -c \end{aligned} \quad (3)$$

The midplane strains are approximated based on the third order polynomials. Dano and Hyer [8] considered the complete third order polynomials and found that the coefficients of the terms with powers of  $x$  and  $y$  that sum to an odd number were always zero. Therefore strains are approximated using the polynomials of Eq. (4).

$$\begin{aligned} \varepsilon_x^0 &= d_1 + d_2x^2 + d_3xy + d_4y^2 \\ \varepsilon_y^0 &= d_5 + d_6x^2 + d_7xy + d_8y^2 \end{aligned} \quad (4)$$

Using Eqs. (1)–(4) and introducing integration constants  $d_{9-11}$ , the in-plane displacements in the  $x$ - and  $y$ -directions,  $u^0$  and  $v^0$ , respectively, can be determined.

$$\begin{aligned} u^0(x, y) &= d_9x + d_{10}y + \frac{1}{2} \left( d_3 - \frac{1}{2}ac \right) x^2y + \left( d_4 - \frac{c^2}{8} \right) xy^2 \\ &\quad + \frac{1}{3} \left( d_2 - \frac{1}{2}a^2 \right) x^3 + \frac{1}{3} d_{11}y^3 \\ v^0(x, y) &= d_{10}x + d_5y + \frac{1}{2} \left( d_7 - \frac{1}{2}bc \right) xy^2 + \left( d_6 - \frac{c^2}{8} \right) x^2y \\ &\quad + \frac{1}{3} \left( d_8 - \frac{1}{2}b^2 \right) y^3 + \frac{1}{3} d_{10}x^3 \end{aligned} \quad (5)$$

The total strain energy of the laminate,  $W$ , can be expressed as

$$W = \int_{vol} \omega d(vol) \quad (6)$$

where the strain energy density,  $\omega$ , is integrated over the volume of the laminate.

$$\omega = \frac{1}{2} c_{ijkl} \varepsilon_{ij} \varepsilon_{kl} - \alpha_{ij} \varepsilon_{ij} \Delta T \quad (7)$$

$c_{ijkl}$ 's are elastic constants,  $\varepsilon_{ij}$ 's and  $\varepsilon_{kl}$ 's the total strains,  $\alpha_{ij}$ 's the thermal expansion coefficients and  $\Delta T$  is the change in temperature. CLT follows the assumption that through-thickness stresses are small in comparison to in-plane-stresses. In assuming a state of plane stress, the normal stress in the  $z$ -direction and out-of-plane shear stresses are assumed to be zero, and expansion of Eq. (6) leads to an expression for the total energy as a function of material and geometric properties, the temperature change and the total strains

$$\begin{aligned} W = & \int_{-L_x/2}^{L_x/2} \int_{-L_y/2}^{L_y/2} \int_{-H/2}^{H/2} \frac{1}{2} \bar{Q}_{11} \varepsilon_x^2 + \bar{Q}_{12} \varepsilon_x \varepsilon_y + \bar{Q}_{16} \varepsilon_{xy} \varepsilon_x + \frac{1}{2} \bar{Q}_{22} \varepsilon_y^2 \\ & + \bar{Q}_{26} \varepsilon_{xy} \varepsilon_y + \frac{1}{2} \bar{Q}_{66} \varepsilon_{xy}^2 - (\bar{Q}_{11} \alpha_x + \bar{Q}_{12} \alpha_y + \bar{Q}_{16} \alpha_{xy}) \varepsilon_x \Delta T \\ & - (\bar{Q}_{12} \alpha_x + \bar{Q}_{22} \alpha_y + \bar{Q}_{26} \alpha_{xy}) \varepsilon_y \Delta T \\ & - (\bar{Q}_{16} \alpha_x + \bar{Q}_{26} \alpha_y + \bar{Q}_{66} \alpha_{xy}) \varepsilon_{xy} \Delta T dx dy dz \end{aligned} \quad (8)$$

where the  $\bar{Q}_{ij}$ 's are the symmetric transformed stiffness matrices [12] of the individual layers,  $L_x$  and  $L_y$  are the planform side lengths of the laminate,  $H$  is the total laminate thickness and the total strains are defined as

$$\begin{aligned} \varepsilon_x &= \varepsilon_x^0 + ZK_x \\ \varepsilon_y &= \varepsilon_y^0 + ZK_y \\ \varepsilon_{xy} &= \varepsilon_{xy}^0 + ZK_{xy} \end{aligned} \quad (9)$$

Substituting Eq. (9) into (8) results in an expression for the total energy of the laminate of the form

$$W = W(a, b, c, d_1, d_2, d_3, d_4, d_5, d_6, d_7, d_8, d_9, d_{10}, d_{11}) \quad (10)$$

To find the minimum energy states it is required that

$$\delta W = \sum_{i=1}^{14} \frac{\partial W}{\partial x_i} \delta x_i = 0 \quad (11)$$

where  $x_i$ 's are  $a, b, c, d_1, \dots, d_{11}$ . To meet this requirement it is necessary to have

$$f_i = \frac{\partial W}{\partial x_i} = 0; \quad i = 1, 2 \dots 14 \quad (12)$$

This results in 14 nonlinear equations to be solved to find the stable room-temperature shapes defined by the 14 constants  $x_i$ . To be a stable solution the Jacobian matrix must also be positive definite.

$$J = \frac{\partial(f_1, f_2 \dots f_{14})}{\partial(a, b \dots d_{11})} \quad (13)$$

Symbolic computing is used to generate the 14 equilibrium equations due to the complex nature of the strain energy density function. A Newton–Raphson approach is then used to solve the system of equations and find the room-temperature shapes. This requires an approximate estimation of the solution. This is achieved by using a known solution for a cross-ply laminate as a starting point. The ply orientations and laminate geometry can then be incrementally changed using the previous solution as the next initial guess to tend towards the solution for the chosen laminate.

### 3. Experimental investigation

This section outlines the experimental work conducted with the aim of characterising the shapes of a series of bistable asymmetric

laminates with arbitrary layup for comparison with shapes predicted by existing modelling methods. This was achieved through a three-dimensional motion analysis technique.

#### 3.1. Laminate manufacture

The experimental study considered five carbon fibre/epoxy composite laminates of differing asymmetric layup:  $[-45/45]$ ,  $[-30/60]$ ,  $[-15/75]$ ,  $[30/60]$ , and  $[45/90]$ . These layups were chosen to provide a range of laminate shapes with differing magnitudes of curvature. All laminates consisted of two plies, each with thickness of 0.25 mm and square edge length of 150 mm. The manufacturing process was a standard layup procedure using M21/T800 carbon fibre prepreg sheet, with properties shown in Table 1.

The laminate was run through a standard autoclave cure cycle with a maximum cure temperature of 180 °C and a pressure of 0.69 MPa. Upon cooling to room-temperature, all five manufactured laminates were observed to have two stable states of curvature. Since the laminate is placed on a flat metallic surface within the autoclave, the side in contact with the surface has a smooth finish while the opposite side has a thin layer of resin which bleeds from the top ply and cures on the surface. Cylindrical shapes with this rough resin layer on the concave surface are denoted as state I while those with the resin layer on the outside convex surface of the cylinder are denoted state II. The effect of this resin layer is discussed later.

#### 3.2. Displacement characterisation

Experimental analysis of the two stable shapes of each of the five laminates was performed to measure the out-of-plane displacement of the laminates. This was carried out utilising standard three-dimensional motion analysis techniques to gain a map of coordinates distributed on the laminate surfaces. Each laminate had 145 round coloured labels of 8 mm diameter attached to one surface (Fig. 3a).

Three digital video camera recorders (Sony DCR-TRV 900E, Sony Corporation, Japan) operating at 50 fields per second were set up in an umbrella configuration [14] around the experimental area. Camera 1 (Fig. 3b) was always positioned to view this area from a high position (the centre of the lens positioned 2.19 m away from the origin of the experimental area at a height of 1.86 m). Due to differences in the shapes of the laminates, the other two cameras were moved such that the best possible viewing angle was always achieved without compromising the umbrella configuration. In total, six different camera set ups were required to capture the 10 different laminate shapes. The other two cameras had the centre of lens ranging from 1.63 to 2.71 m away from the origin in different set ups with the height ranging from 0.51 to 1.32 m above the experimental area. The height and locations of cameras varied in such a way that the cameras were not all in the same plane in accordance to recommendations by Nigg et al. [14]. The angle between the cameras ranged from 55 to 105° with a mean angle

**Table 1**  
M21/T800 prepreg sheet properties [13].

Property	Value
Longitudinal Young's modulus, $E_{11}$ (GPa)	157.0
Transverse Young's modulus, $E_{22}$ (GPa)	8.5
Poisson's ratio, $\nu_{12}$	0.35
Shear modulus, $G_{12}$ (GPa)	4.5
Longitudinal thermal expansion coefficient, $\alpha_1$ ( $\times 10^{-6}/^\circ\text{C}$ )	-0.09
Transverse thermal expansion coefficient, $\alpha_2$ ( $\times 10^{-6}/^\circ\text{C}$ )	30.0

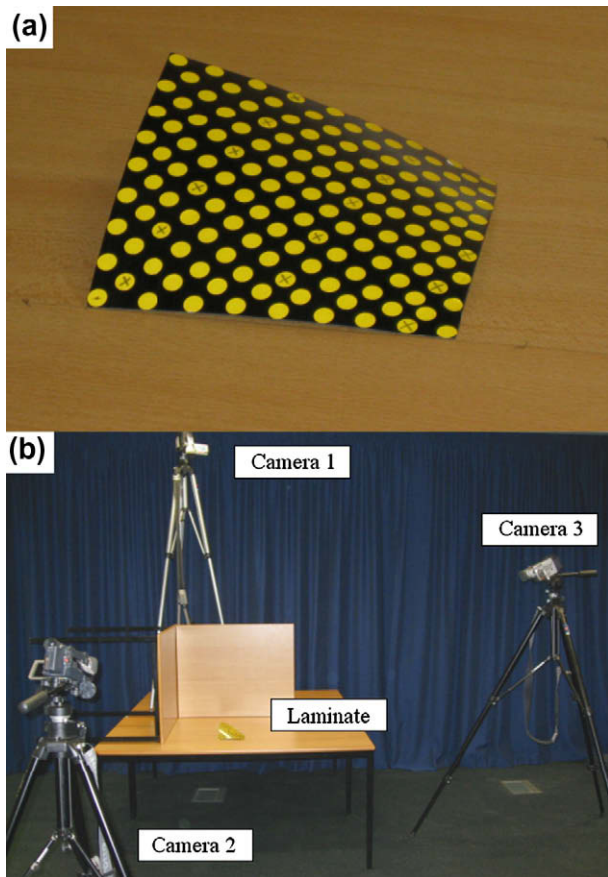


Fig. 3. (a) Round labels distributed on the surface of a square  $[45/90]$  laminate and (b) an example of experimental camera setup.

between the three cameras varying from  $77$  to  $92^\circ$  in different set ups.

The laminates were positioned within the experimental volume, which was calibrated with a  $200 \times 200 \times 100$  mm wire frame. The camera views were restricted to a volume just slightly larger than the calibration frame. The wire frame was videotaped in each camera set up before it was removed and the laminate was positioned within this calibrated volume. Following this, the laminates were videotaped simultaneously by the three video cameras.

Mapping of the surface co-ordinates was carried out using Peak-Motus motion analysis system (v. 8.5, Vicon, USA) after transferring the calibration and laminate video clips onto the computer. First, the eight corners of the calibration wire frame were manually digitised from each camera view (and for each camera set up). Then, the centre of each of the 145 round labels and the four corners of the each laminate were manually digitised from all three camera views using a round cursor matching the size of the round labels. The digitised area was  $1440 \times 1152$  pixels.

Due to the curved shape of the laminates, it was not always possible to see every label or corner point of the laminate from all cameras. The minimum requirement to get a three-dimensional co-ordinate is that the point is visible for at least two cameras, which was the case for all points. In most laminates, all the points were visible for all three cameras. In those occasions when all points were not visible, the maximum number of non-visible points was five in one view.

The digitised pixel information from each camera view was combined with the calibration information to transform these to Cartesian co-ordinates of the laminate surfaces using Direct Linear

Transformation method [15]. The mean of the RMS error of six different set ups between the known eight calibration co-ordinates and the respective digitised points were  $0.2$  mm for each co-ordinate direction.

#### 4. Results and discussion

The measured Cartesian co-ordinates of each of the 10 laminate shapes were three-dimensionally rotated to match the co-ordinate system defined for the analytical model using Matlab<sup>®</sup>. This was because the experiments were set up in such a way to capture the most data points of laminates, each of which has different three-dimensional curvatures. The centre of both laminates was then set to  $[0, 0, 0]$  such that the  $z$ -co-ordinates of the experimental points represent the out-of-plane displacements of the laminate and the lines of symmetry in the curvatures were aligned to determine the angle of rotation about each of the three axes. Surface fitting was applied to the transformed data using the method outlined in [16]. This spline interpolation method fits a surface of the form  $z = f(x, y)$  to the non-uniformly spaced data and interpolates this surface at the uniformly specified mesh grid points. The fitted surface is then plotted alongside the shape predicted by the analytical model. An example plot of state I of the  $[-45/45]$  laminate is shown in Fig. 4, including both the mesh fit and individual data points. The surface generated using the experimental data is offset for illustrative purposes.

The analytical models of the  $[0 \pm \theta/90 \pm \theta]$  laminate family have two stable shapes of equal and opposite curvature. For square laminates of this type, if the laminate is inverted it can be oriented in the  $x$ - $y$  plane such that the layup definition remains unchanged. This results in the prediction of two identical shapes of different global orientation. Such behaviour is observed for the  $[-45/45]$ ,  $[-30/60]$ ,  $[-15/75]$  and  $[30/60]$  laminates. However, this is not the case for the  $[45/90]$  laminate where two stable shapes of both different angle of principal curvature and magnitude of curvature are observed. The two observed shapes, and those predicted, are shown in Fig. 5. Experimental data is again offset.

The analytical model and experimental shapes generally show good agreements for all laminates studied and the  $[-45/45]$  laminate is presented as a demonstrative example in Fig. 4. This is more closely examined in Figs. 6 and 7 where the curvature profiles in the major and minor axes,  $C$ - $D$  and  $A$ - $B$ , respectively, are plotted. These profiles are selected as the errors at the corners are at their maximum, as shown in Table 2. As the reference point for the comparison is set at the centre of the laminates, the error at the centre is zero. The profiles in the major axis of Fig. 6 show that the profiles for both states are smooth and the curvature deviation increases smoothly towards the corners of the laminates. The discrepancies

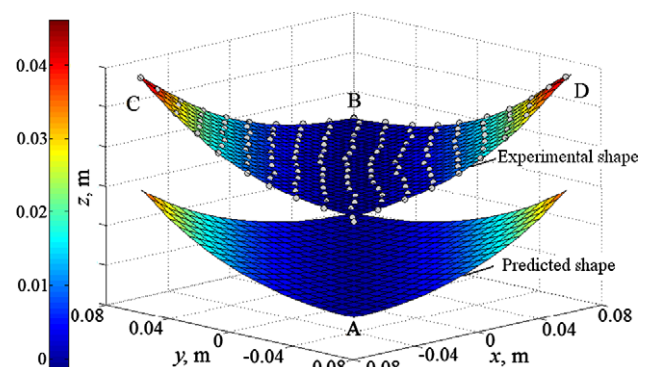


Fig. 4. Predicted room-temperature state I cylindrical shape and experimental data with spline fitted surface for square  $[-45/45]$  laminate. Experimental data offset.

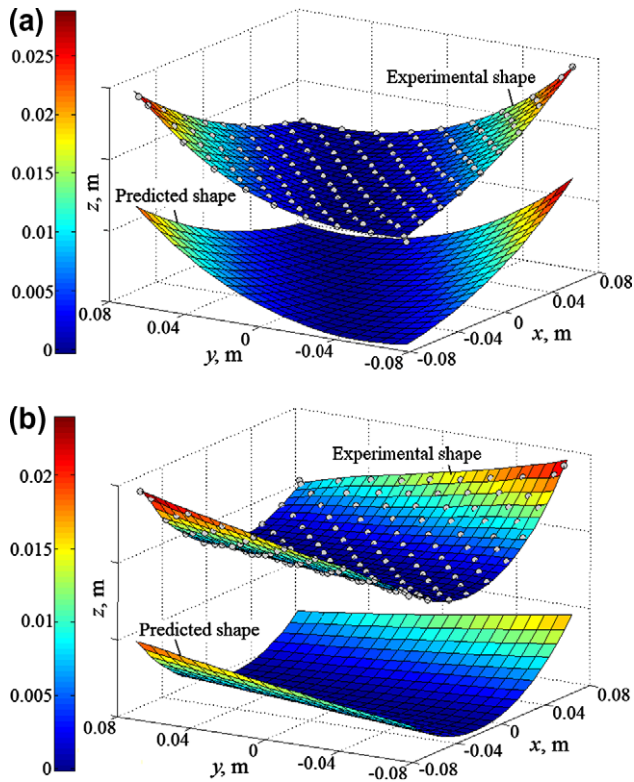


Fig. 5. Predicted shapes and offset experimental data of square [45/90] laminate: (a) state I cylindrical shape and (b) state II cylindrical shape.

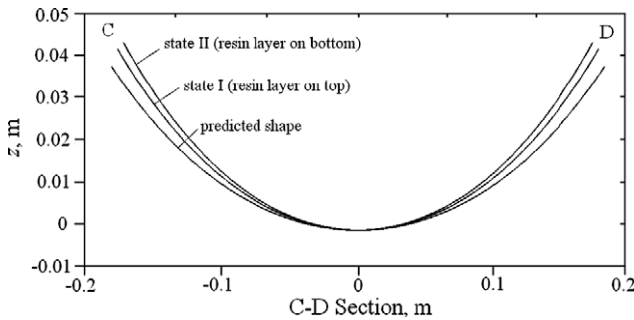


Fig. 6. Cross-section profile of experimental and predicted shapes of [-45/45] laminate along line C-D.

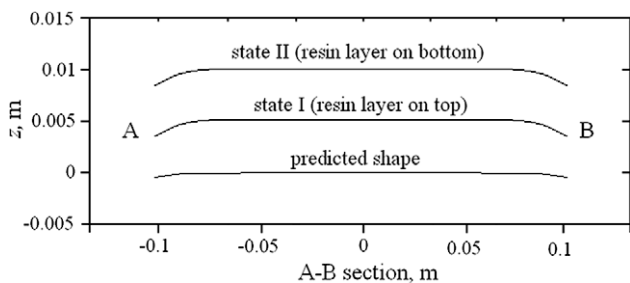


Fig. 7. Cross-section profile of predicted and offset experimental shapes of [-45/45] laminate along line A-B.

in the curvatures between states are also noticeable which the analytical model does not take into account.

Table 2

Experimental and predicted maximum out-of-plane displacements. II-I corresponds to the difference between States I and II.

Laminate	State	Maximum out-of-plane displacement (mm)			Error (%)	
		Predicted (ideal)	Predicted (resin)	Experimental	Ideal	Resin
[-45/45]	I	38.05	37.25	42.69	-10.9	-12.7
	II	38.05	37.99	43.39	-12.2	-12.4
	II-I	0.00	0.74	0.70	1.3	0.3
[-30/60]	I	35.51	34.76	38.14	-6.9	-8.9
	II	35.51	35.45	41.24	-13.9	-14.0
	II-I	0.00	0.69	3.10	7.0	5.1
[-15/75]	I	28.55	27.95	29.29	-2.5	-4.6
	II	28.55	28.50	31.67	-9.9	-10.0
	II-I	0.00	0.55	2.38	7.4	5.4
[45/90]	I	26.61	24.76	27.77	-4.2	-10.8
	II	19.03	19.29	22.85	-16.7	-15.6
	II-I	-7.58	-5.47	-4.92	12.5	4.8
[30/60]	I	14.63	12.56	12.77	14.6	-1.6
	II	14.63	15.94	15.09	-3.0	5.6
	II-I	0.00	3.38	2.32	17.6	7.2

Fig. 7 shows the curvature profile along the minor axis. Here, the deflections for the analytical model show only a slight anticlastic curvature. The experimental data show near zero deflections in the non-boundary region but pronounced high curvatures near the boundaries. This clearly demonstrates that free edge characteristics around the boundaries affect just over 10% of the overall dimension. The existence of the free edge effects is well known [17] and this has not been included in the analytical model. The free edge effects are discussed further in Section 4.3.

The maximum errors at the corners for each of the 10 laminate shapes at states I and II are summarised in Table 2. As the analytical model predicts the same curvature for both states while each state have different curvatures in practice; the difference between two state curvatures (II-I) are also included in Table 2. In order to quantify the effect of a thin resin layer, a layer with the properties of the cured resin [11] is added to the analytical model and discussed in Section 4.1. The percentage error represents the predicted maximum out-of-plane displacement minus the measured displacement. The factors attributing to the errors are examined more closely in the following sections.

4.1. Effect of additional resin layer

One distinct characteristic of these results is the consistent effect of the thin resin layer. All laminates of the  $[0 \pm \theta/90 \pm \theta]$  family were found to have larger out-of-plane displacement in state II, compared to state I, with the rough resin layer on the convex surface (Table 2). As this layer is not included in the analytical model the two states are predicted to have equal magnitudes of maximum displacement. The laminate profile of Fig. 6 shows that the difference in shape is not negligible between state I and II as discussed earlier. The difference in maximum out-of-plane displacement between states for this family of laminates was found to vary by between 0.7 and 3.1 mm leading to differences in errors between states of 1.3–17.6%.

A thin layer of cured epoxy resin is added to the analytical model to quantify its effect. Images of the cross-section from optical microscopy of one example laminate are used to investigate the thickness of this additional layer [11]. It is found that far from having a uniform thickness the resin layer varies from negligible to

0.08 mm across the entire surface. A mean thickness of 0.025 mm is taken to be representative of this layer and this approach has been used in a FE model to achieve good accuracy [11].

The effect of modelling an additional resin layer is shown in Table 2. Where previously it had been predicted that state I and state II should have equal maximum out-of-plane displacements, the shapes with a resin layer show the differential curvatures as seen in the experimental results. The state with the largest displacement agrees with experimental results for all laminates. The differences in the predicted maximum out-of-plane displacement between states for the  $[0 \pm \theta/90 \pm \theta]$  family of laminates are found to vary by between 0.7 and 3.4 mm, correlating well with experimental results. This additional layer in the model leads to differences in errors between states of 0.3–7.2%, a significant improvement over the ideal model.

It is also noted that a thin layer of resin exists between the plies. This layer is observed to be of the order of 100th of a ply thickness so the effect on the overall laminate shape is small. Inclusion of a resin layer between plies in the analytical model showed that a layer of one twentieth of a ply thickness is required for a 1% variation in maximum displacement. This effect is clearly less than that of the surface resin layer, but can be significant for a different manufacturing process.

#### 4.2. Effects of ply thickness

In the ideal modelling case it is also assumed plies are uniform both in terms of geometry and material properties. Hamamoto and Hyer [3] found that slight imperfections as little as 1% in the thickness of each layer of the laminate can cause the bifurcation behaviour to disappear and significantly affect temperature–curvature relationship.

The microscopy images of the laminate sections suggest it is reasonable to expect  $\pm 2\%$  variation in the thicknesses of individual plies as a result of variability during manufacturing. The effect of these potential imperfections is investigated by modelling each of the laminates with a through-thickness profile of  $[t + 2\%/t - 2\%]$ , where  $t$  is the ideal single ply thickness. This imperfection is found to lead to changes in maximum out-of-plane displacement for the 10 laminate shapes of up to  $\pm 4.6\%$ . Given the magnitudes of the errors in Table 2 this thickness effect is significant.

#### 4.3. Free edge characteristics

Fig. 7 depicts the profiles of the predicted and experimental shapes along the minor curvature A–B (see Fig. 4), for the  $[-45/45]$  laminate. This trend was observed in all laminates tested where the out-of-plane displacement is small across the central region but increases significantly at the edges. It is well known that interlaminar stresses increase rapidly near free edges of laminates and this leads to the high out-of-plane displacement observed in Fig. 7 [17]. As the interlaminar stresses are not included in the analytical model, this high out-of-plane displacement is only observed in the experimental data.

In-plane interlaminar stress arises from the mismatch of thermal expansion coefficients between plies. In order to satisfy boundary conditions at the free edges, the overall in-plane direct stresses of the laminate must be zero. This leads to increased through-thickness stresses along the edges of the laminate, hence the high out-of-plane displacement [18]. It follows that the magnitude of the displacement is dependent on the ply orientations [19]. It has been suggested that the combination of two adjacent free edge effects further increases the displacement at the corners [18]. This free corner effect is observed in the sudden curvature change and the peak displacement in Fig. 7.

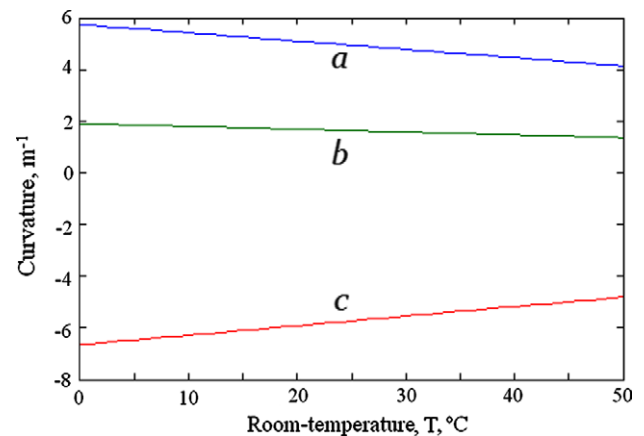


Fig. 8. Variation in curvature with temperature for  $[-45/45]$  laminate.

#### 4.4. Temperature dependency

The bistable configuration arises from the anisotropic thermal expansion of the composite materials (Table 1). As a result the dependency of the bistable laminate shapes to the cure and ambient temperatures must be quantified. The relationship between temperature and curvature is well documented [8] and the sensitivity can be easily investigated using the existing analytical model. Away from the bifurcation point the temperature–curvature relation is approximately linear. With reference to Eq. (1), the three shape constants defining the out-of-plane displacement of the  $[-45/45]$  laminate,  $a$ ,  $b$ , and  $c$ , are modelled to vary with temperature as shown in Fig. 8.

The predicted shapes of the laminates are generated using a standard room-temperature value of 21 °C. Any variation in temperature when obtaining the experimental data will affect the measured curvatures. It is reasonable to assume that there is some variability in the quoted cure temperature of 180 °C. Equally, the room-temperature around the experimental test area cannot be guaranteed consistent. Using the relationships shown in Fig. 8, as little as 5 °C difference in the temperature change corresponds to a change in maximum deflection of around 3% of the total deflection when compared with the quoted modelling values. A similar magnitude was observed for all laminates. Potential temperature dependent discrepancy is significant. This result highlights the sensitivity of the model to physical conditions. Other environmental effects such as moisture content [20] and variability in prepreg material properties over time may also be significant in the long term.

### 5. Conclusions

This paper investigates analytical modelling of bistable composite laminates with arbitrary layup through a novel technique of mapping the surface. The  $[0 \pm \theta/90 \pm \theta]$  family of laminates tends to have stable shapes of equal and opposite curvature. The total error between predicted and measured maximum deflections varied between 2.5% and 16.7%. The results reveal that the solutions are sensitive to imperfections such as resin layers, ply thicknesses, free edge effects and temperature effects. Investigation of the sensitivity of displacement to ply and resin layer thicknesses can typically account for 5% error. Sensitivity of displacement to temperature has shown that as little as 5 °C variability in the cure or ambient temperatures can result in a further 3% change in total displacement. Inclusion of sensitivity analysis and non-uniform properties of individual plies is proposed in the development of a design tool

for laminates of this type. The work presented here indicates that existing modelling methods are of use for the design of bistable composite structures of arbitrary layup for shape change applications; however full experimental characterisation of factors identified in this paper is desirable.

## References

- [1] Hyer MW. Some observations on the cured shape of thin unsymmetric laminates. *J Compos Mater* 1981;15(March):175–94.
- [2] Hyer MW. Calculations of the room-temperature shapes of unsymmetric laminates. *J Compos Mater* 1981;15(July):296–310.
- [3] Hamamoto A, Hyer MW. Nonlinear temperature–curvature relationships for unsymmetric graphite-epoxy laminates. *Int J Solids Struct* 1987;23(7):919–35.
- [4] Jun WJ, Hong CS. Effect of residual shear strain on the cured shape of unsymmetric cross-ply thin laminates. *Compos Sci Technol* 1990;38(1):55–67.
- [5] Ren L, Parvizi A, Li Z. Cured shape of cross-ply composite thin shells. *J Compos Mater* 2003;37(20):1801–20.
- [6] Dang J, Tang Y. Calculation of the room-temperature shapes of unsymmetric laminates. In: *Proceedings of the international symposium on composite materials and structures*; 1986. p. 201–6.
- [7] Jun WJ, Hong CS. Cured shape of unsymmetric laminates with arbitrary lay-up angles. *J Reinf Plast Compos* 1992;11(12):1352–66.
- [8] Dano M-L, Hyer MW. Thermally induced deformation behavior of unsymmetric laminates. *Int J Solids Struct* 1998;35(17):2101–20.
- [9] Dano M-L, Hyer MW. SMA-induced snap-through of unsymmetric fiber-reinforced composite laminates. *Int J Solids Struct* 2003;40(22):5949–72.
- [10] Ren LB. A theoretical study on shape control of arbitrary lay-up laminates using piezoelectric actuators. *Compos Struct* 2008;83(1):110–8.
- [11] Giddings PF, Bowen CR, Salo AIT, Kim HA. Bistable composite laminates: effects of laminate composition on cured-shape and response to thermal load. *Compos Struct.*, in press. doi:10.1016/j.compstruct.2009.08.043.
- [12] Matthews FL, Rawlings RD. *Stiffness of unidirectional composites and laminates*. In: *Composite Materials: Engineering and Science*. London: Chapman and Hall; 1994. p. 223–50.
- [13] Hexcel Corporation. HexPly Prepreg Selector Tool. <<http://www.hexcel.com/Products/Selector+Guides>>.
- [14] Nigg BM, Cole GK, Wright IC. Optical methods. In: Nigg BM, Herzog W, editors. *Biomechanics of the musculo-skeletal system*. Chichester, UK: John Wiley & Sons; 2007. p. 362–91.
- [15] Abdel-Aziz YI, Karara HM. Direct linear transformation from comparator coordinates into object space coordinates in close-range photogrammetry. In: *Proceedings of the ASP/IU symposium on close-range photogrammetry*; 1971. p. 1–118.
- [16] Sandwell DT. Biharmonic spline interpolation of GEOS-3 and SEASAT altimeter data. *Geophys Res Lett* 1987;14(2):139–42.
- [17] Kant T, Swaminathan K. Estimation of transverse/interlaminar stresses in laminated composites – a selective review and survey of current developments. *Compos Struct* 2000;49(1):65–75.
- [18] Mittelstedt C, Becker W. Interlaminar stress concentrations in layered structures: part 1 – a selective literature survey on the free-edge effect since 1967. *J Compos Mater* 2004;38(12):1037–62.
- [19] Nosier A, Maleki M. Free-edge stresses in general composite laminates. *Int J Mech Sci* 2008;50(10–11):1435–47.
- [20] Etches J, Potter K, Weaver P, Bond I. Environmental effects on thermally induced multistability in unsymmetric composite laminates. *Compos Part A – Appl Sci Manuf* 2009;40(8):1240–7.